

NASA TECHNICAL NOTE



NASA TN D-5237

c.1

NASA TN D-5237



LOAN COPY: RETURN TO
AFWL (WLIL-2)
KIRTLAND AFB, N MEX

DESIGN CONSIDERATIONS FOR CYCLOTRON RESONANCE OSCILLATORS

by Bernhard Kulke

*Electronics Research Center
Cambridge, Mass.*



DESIGN CONSIDERATIONS FOR
CYCLOTRON RESONANCE OSCILLATORS

By Bernhard Kulke

Electronics Research Center
Cambridge, Mass.

NATIONAL AERONAUTICS AND SPACE ADMINISTRATION

For sale by the Clearinghouse for Federal Scientific and Technical Information
Springfield, Virginia 22151 - CFSTI price \$3.00

ABSTRACT

From the linearized kinetic theory of stimulated cyclotron radiation, and from related physical arguments, some design criteria are deduced for spiraling-beam cyclotron-resonance oscillators for possible use at millimeter-wave frequencies. While an optimum choice of the geometry of the interaction region is important, the most essential design problem is the control and minimization of the axial velocity spread on the spiraling beam.

DESIGN CONSIDERATIONS FOR CYCLOTRON RESONANCE OSCILLATORS

By Bernhard Kulke
Electronics Research Center

SUMMARY

Recent work on periodic-beam microwave devices has indicated that these devices show some promise for development into powerful, tunable sources in the millimeter and submillimeter wavelength range. However, no comparative evaluation of different designs has been attempted to date. In this report, some design criteria are deduced for spiraling-beam cyclotron-resonance oscillators, based on the linearized kinetic theory of stimulated cyclotron radiation and on related physical arguments. In the absence of limiting-amplitude calculations, the start-oscillation current is used as an indicator of device activity and, hence, a qualitative predictor of efficiency. It is shown that while an optimum choice of the geometry of the interaction region is important, the most essential design problem is the control and minimization of the axial velocity spread of the spiraling beam.

INTRODUCTION

Cyclotron resonance oscillators are devices where an ensemble of mono-energetic electrons, orbiting in a uniform magnetic field, are stimulated by an rf electric field to emit coherent radiation. This is not to be confused with the spontaneous (and generally incoherent) radiation of accelerated classical charges (see Appendix A). Several different devices of this class have been demonstrated recently, both with spiraling electron beams (refs. 1-5) and with cycloidal sheet beams (ref. 6). These devices show some promise for development into powerful, tunable sources in the millimeter and submillimeter wavelength range. As such, they would help to open up a range of the electromagnetic spectrum that until now has not been very useful for communications because of a lack of powerful sources.

The purpose of this report is to serve as a summary of work done to date on an in-house project at the Electronics Research Center, which is aimed at a broad engineering evaluation of cyclotron resonance devices. In particular, it is desired to assess the inherent limitations, if any, on power output, efficiency, and frequency, and in the process to derive information that will result in optimum design. The theoretical work is complemented by experimental data designed to verify certain predictions and improve the understanding of the physical phenomena taking place.

SYMBOLS

| | |
|------------------------|--|
| u_0 | axial beam velocity in the interaction region |
| w_0 | transverse beam velocity in the interaction region |
| p_c | corkscrew pitch |
| ω_b | cyclotron frequency |
| $e/m \equiv \eta$ | charge-to-mass ratio |
| μ_0 | permeability of free space |
| I | current |
| r_c | corkscrew radius |
| u | axial beam velocity at some point along the axis |
| w | transverse beam velocity |
| d_0 | linear beam diameter at cathode |
| d_1 | linear beam diameter after compression |
| B_0 | axial magnetic field linking the cathode |
| B_1 | axial magnetic field at some point along the axis |
| B_\perp | transverse magnetic field |
| D | total beam diameter |
| r_b | cyclotron radius |
| \vec{J} | ac current density |
| \vec{E} | rf electric field vector |
| k_\parallel, k_\perp | axial and transverse components of the wave vector |
| I_0 | dc beam current |
| ω | radian frequency of rf cavity fields |
| U | energy stored in cavity |
| Q_L | loaded Q |

| | |
|------------------|--|
| τ | transit time |
| Q_0 | unloaded (internal) Q |
| Q_{ext} | external Q |
| R_{sh} | equivalent shunt resistance of cavity |
| G_{sh} | equivalent shunt conductance of cavity |
| G_e | equivalent electronic beam-loading conductance |
| V | rf voltage drop along electron trajectory |
| b | beam clearance in cavity |
| Ω | relativistic cyclotron frequency |
| m_0 | electron rest mass |
| γ | relativistic mass change parameter |

REVIEW OF PREVIOUS WORK

Cyclotron resonance oscillators have had a variety of experimental embodiments, and some of these designs are summarized briefly in Table I. As might be expected, the design of a prototype model in connection with the in-house work, drew heavily on the information contained in Table I. Two design decisions are basic: the choice of the beam trajectory, and the choice between resonant or backward-wave interaction. A simple helical beam, generated by a magnetic corkscrew, was chosen for its relative simplicity and precise controllability in the laboratory.

From Table I, it is evident that devices based on backward-wave interaction have generally shown greater efficiency than resonant-cavity devices. However, the former require a longer region of homogeneous magnetic field. Thus, in the absence of any analytical evidence that backward-wave devices are inherently more efficient, it was decided for the in-house experiment to take advantage of the economy in magnetic-field volume offered by the resonant-cavity approach.

The basic operation of a helical-beam cyclotron resonance oscillator is described in Figure 1. An electron beam is formed by a triode gun that is immersed in an axial magnetic field of two to three times the Brillouin value. A small transverse magnetic field component forces the electrons into slightly spiraling trajectories, and the beam then drifts axially into a

TABLE I

COMPARISON OF EXPERIMENTAL PARAMETERS FOR SOME CYCLOTRON RESONANCE OSCILLATORS

| Experiment | Bott (ref. 1) | Hirshfield Bernstein and Wachtel (ref. 2) | Gaponov, et al. (ref. 4) | Schriever and Johnson (ref. 3) | Antakov, et al. (ref. 6) | Kulke and Wilmarth (ref. 7) |
|-------------------------------------|--|--|-------------------------------------|--------------------------------------|--------------------------------|--|
| Type of gun | Pierce gun immersed | Parallel-plane diode, immersed | Conical cathode | Magnetron injection gun | Kino gun | Pierce gun immersed |
| Electron trajectory | Spiral | Spiral | Spiral | Spiral | Cycloid | Spiral |
| Beam voltage | 20 kV | 5 kV | 19 kV | 10 kV | 14 kV | 15 kV |
| Cathode current | 25 mA | 50 mA | 320 mA | 1300 mA | 600 mA | 25 mA |
| Type of trajectory modulation | Corkscrew | Corkscrew | Crossed-field injection | Crossed-field injection | Crossed-field injection | Corkscrew |
| Mirror ratio | ≤ 170 | 7.5 | - | 6 | 6-8 | 10 |
| Type of interaction | Combination resonant and backward-wave Circular TE_{mn} | Resonant, circular TE_{011} | Resonant, circular TE_{021} | Backward-wave | Backward-wave | Resonant, rectangular TE_{101} |
| Power | 1 W | 10 mW | 190 W | 720 W | 850 W | 4.2 W |
| Frequency | 143 GHz | 5.8 GHz | 25 GHz (2nd harmonic) | 9 GHz | 38 GHz | 9.6 GHz |
| Efficiency* | 2% | - | 3% | 6% | 10% | 1% |

*Some ambiguity exists depending on whether cathode or collected current should be used as a base. Here, cathode current is used.

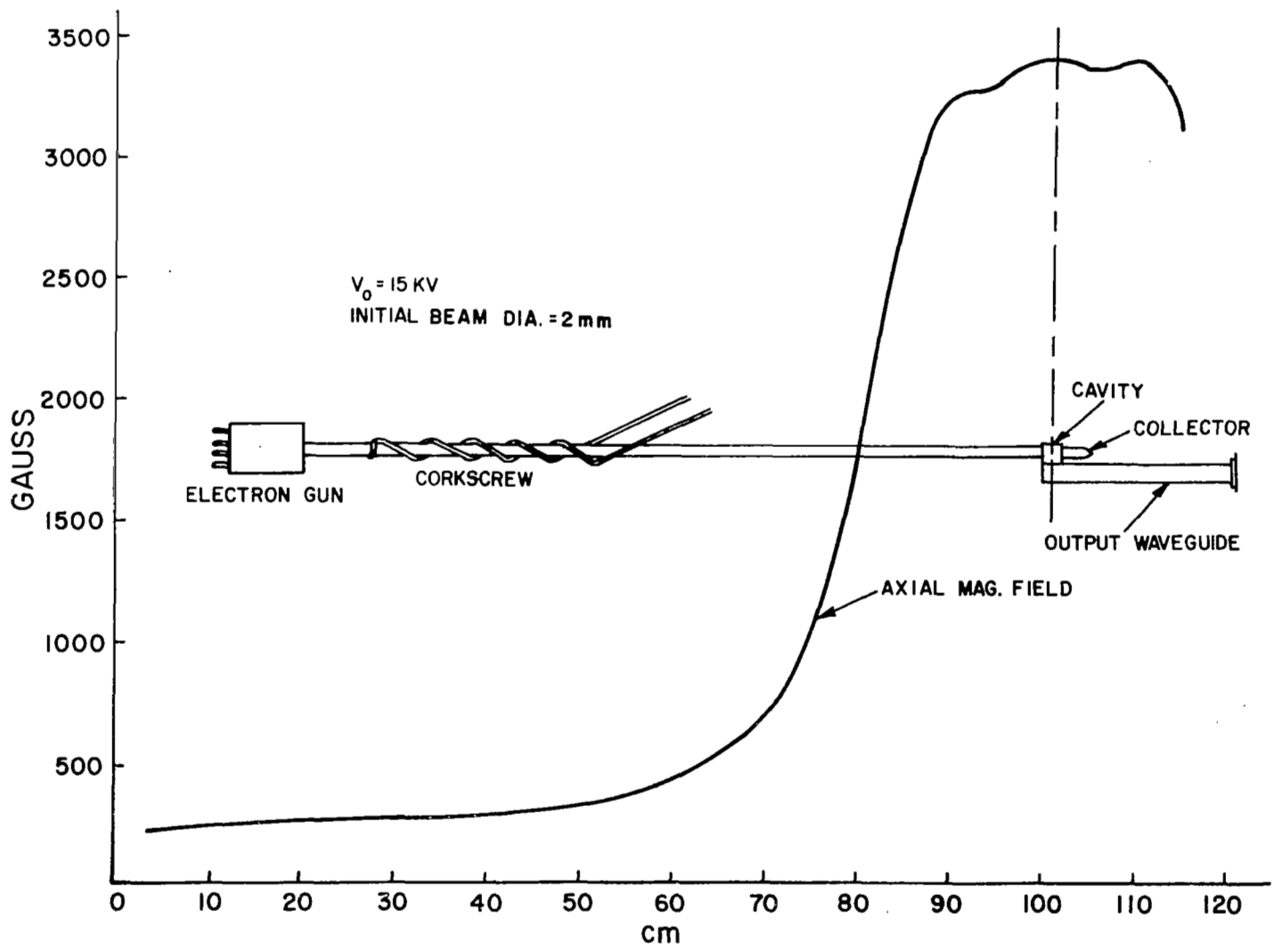


Figure 1.- Experimental cyclotron resonance oscillator, shown to scale with axial magnetic field profile.

region of increasing magnetic field, where more and more axial kinetic energy is transformed into transverse energy. Once the beam reaches the point where nearly all its momentum is in the transverse direction, it drifts into a microwave cavity that is resonant in a TE mode slightly above the cyclotron frequency of the orbiting electrons. Within a narrow range of drift velocity and magnetic field, this resonance will couple to the spiraling beam, and gain or oscillations are obtained. The spent beam is then collected. Power is coupled from the cavity through an iris into the waveguide output.

Throughout this report, the small-signal interaction between the spiraling beam and the electromagnetic field is discussed in terms of the linearized kinetic theory used by Hirshfield, Bernstein, and Wachtel (ref. 2). Other approaches are possible and have been pursued elsewhere. One of these is the Pierce-type analysis (ref. 8) which was used, for example, by Chow and Pantell (ref. 9) in their analysis of a traveling-wave spiraling-beam device. In this method, one describes first the rf modulation on the beam due to the circuit fields, then the circuit fields induced by the beam perturbation, and finally one requires the two expressions to be consistent. The resulting dispersion relation is formidable, but with the aid of a high-speed computer it can be solved numerically for the complex propagation constants. The small-signal gain and the start-oscillation conditions can then be calculated by imposing appropriate boundary conditions. Two different physical mechanisms have been identified which may cause the necessary bunching (phase-focusing) of the orbiting electrons into a decelerating phase in the transverse electric fields of the rf cavity. Chow and Pantell based their analysis on one such mechanism where the dc rotation of the electrons and the transverse ac magnetic field of a traveling wave produce a z-directed Lorentz force, and this tends to bunch electrons into the decelerating phase of the traveling transverse electric field vector of the waveguide. This process will hereafter be called "Pantell bunching." However, a phase-focusing effect can also arise from the relativistic mass change of the orbiting electrons. If the orbiting electrons are initially assumed to have random phases, then those with initial phases such as to gain energy from the rf fields become heavier and accumulate phase lag, and those with initial phases such as to lose energy to the rf fields become lighter and accumulate phase lead. Sehn (ref. 10) re-derived the dispersion relation applicable to backward-wave interaction in relativistic form, and he concluded that the relativistic bunching mechanism is roughly as effective as the Pantell bunching, and, therefore, cannot be neglected.

In recent experiments at the University of Utah (ref. 11), both forward and backward traveling-wave interaction have been observed, and were clearly distinguishable in terms of frequencies.

In addition, a third mode of interaction occurred at a frequency halfway between the other two modes, which was labeled the cyclotron resonance mode, but this mode was not analyzed further.

Although the Utah group did not consider any relativistic bunching effects, their theory did allow them to identify accurately beam interaction with the forward or backward traveling waveguide modes. Their theoretical prediction of start oscillation current has not been verified accurately by experiment, however, and thus it is difficult to tell at this time what quantitative effect, if any, their neglect of relativistic effects does have. A clear confirmation or refutation of Sehn's conclusion, therefore, does not yet exist.

It is of interest to compare the theoretical synchronism conditions that apply to traveling-wave and standing-wave interaction. Interaction between the beam spiraling with gyrofrequency, Ω , and the forward-traveling circuit wave of frequency, ω , requires that

$$\omega = \Omega + k_{\parallel} u , \quad (1)$$

where k_{\parallel} and u are the axial propagation constant and the axial beam velocity, respectively (ref. 11). As will be shown later in the section discussing the gain function, an almost identical synchronism condition exists for the standing-wave interaction,

$$\omega = \Omega - x k_{\parallel} u \quad (2)$$

where $x \approx (-0.85)$ corresponds to the desired condition of peak negative beam loading of the cavity. The standing-wave interaction frequency, therefore, would be expected to differ only slightly from that for the forward-traveling wave interaction. One is led to the intuitively appealing conclusion that the standing-wave interaction actually takes place selectively with one of the component traveling waves. An experimental confirmation of this conclusion, however, is not yet available. Tied in with this problem is the unanswered question of whether traveling- or standing-wave interaction leads to a basically more efficient device.

In Pierce's original analysis of beam-wave interaction (ref. 8), the coupling between the normal modes of a beam and of a waveguide is considered implicitly, as certain propagation constants are dropped from the dispersion relation. A more explicit coupled-mode formalism was developed later, first for

a linear beam (ref. 12) and then for a beam executing transverse motion under the influence of rf forces (ref. 13).

This coupled-mode formalism has been applied extensively, for example, by the Utah group (ref. 11) in their thorough follow-up to Chow and Pantell's work on transverse traveling wave devices.

McIsaac (ref. 14) has derived a relativistically correct set of coupled-mode equations, based on the six normal modes of a beam with spiraling dc motion. This work also is still in progress, and no correlation with experimental data has so far been attempted.

An important advantage of the coupled-mode formalism is its capability to identify possible beam-circuit interaction modes. To proceed from the coupled-mode expressions to tractable engineering formulas, e.g., for the start-oscillation current, however, seems to be relatively difficult.

A somewhat different approach was taken by Hsu and Robson (ref. 15) who analyzed the spiraling-beam interaction with a Cuccia coupler by assuming a small rf perturbation on the dc electron velocity vector and carrying this directly through the non-linear, relativistic equation of motion. This approach was later extended by Hsu (ref. 16) to include beam interaction with the transverse electric fields of a resonant cavity. With suitable assumptions, Hsu was able to get good agreement with the start-oscillation currents measured earlier by Bott (ref. 1). However, these assumptions involve the ratio of transverse to axial velocity which, although crucial to the result, is very difficult to verify experimentally.

In fact, the lack of accurate knowledge of the axial velocity and of the velocity spread in the interaction region appears to plague all predictions of start-oscillation current, regardless of the theory on which they are based. In this sense, the distinctions between the different theories become almost irrelevant, because any of them only provide rough predictions of the start-oscillation current.

Further experimental work which should also be mentioned is the device built by H. Jory (ref. 17), where an initially linear, 0.100 inch diameter, beam is injected into an X-band accelerator cavity driven with up to 75 kW of pulsed power. The beam emerges from this cavity in a spiraling trajectory with a kinetic energy of 300-500 keV (mainly transverse), and then enters axially into a cylindrical $TE_{n,1,1}$ ("barrel") resonator. As the beam spirals through the cavity, almost grazing the wall, it will interact with the tangential component of the periodic rf electric field

patterns in what closely approximates conventional linear-beam periodic-field type interaction. The combination of the very high beam velocity and the overmoding of the cavity (up to $n = 14$) has enabled the device to operate at nearly 10 times the electron cyclotron frequency, with outputs up to 6 W at 84 GHz. The spiraling trajectory of Jory's beam could lead one to attempt an analysis of his device in terms of Pantell-type or relativistic bunching, but the approach followed by Jory, in terms of conventional bunching along the circumference, is clearly more appropriate. Thus, this tube really is not a cyclotron resonance device.

As has been mentioned previously, the small-signal kinetic-theory approach as used by Hirshfield, Bernstein, and Wachtel (ref. 2) will be followed in this report. This approach is borrowed from the realm of plasma physics, as it involves solving the collisionless Boltzmann equation, and it is definitely limited to the small-signal regime, e.g., the prediction of electronic gain and of start-oscillation currents. It is attractive because of its algebraic compactness and because it automatically takes into account both the relativistic and the Pantell-type bunching. Also, the kinetic-theory approach in principle yields solutions for any given electron velocity distribution. This latter capability is important, as both theory and experiment indicate that the width of this distribution constitutes perhaps the most important design characteristic of a cyclotron resonance oscillator.

Some problems encountered in generating a beam having the desired narrow velocity distribution are discussed in the following section.

FORMATION OF A SPIRALING ELECTRON BEAM

The choice of beam geometry and the manner in which the beam is generated have a profound effect on the operation of cyclotron resonance devices because both affect the velocity distribution of the electrons interacting with the cavity fields. In Table I, a comparison has already been made between the pertinent design data for some experimental devices. A tremendous amount of work has been done by many authors in the field of electron optics, and no attempt will be made here to provide a comprehensive evaluation of different gun systems suitable for spiraling-beam oscillators at a given power level and frequency.

The design to be discussed here already has been mentioned in connection with Figure 1. The transverse perturbation is of the order of one percent of the axial field and is set up by a "corkscrew" magnetic field (ref. 18) that is generated by a

current-carrying bifilar helix wound externally around the non-magnetic, evacuated drift tube. The length of this helix is somewhat arbitrary, but there is an obvious trade-off between the length and the helix current. The transverse magnetic field vector is screw-symmetric along the beam and thus forces the electrons into slightly spiraling trajectories with pitch identical to that of the corkscrew, and the fraction of axial kinetic energy so converted into transverse energy will depend on the corkscrew length and on the current. The corkscrew pitch p_c follows from the synchronism requirement

$$\frac{p_c(z)}{u(z)} = \frac{2\pi}{\omega_b} \quad (3)$$

where $u(z)$ = axial beam velocity, a function of distance, and $\omega_b = (e/m)B_{\perp} =$ cyclotron frequency. As the axial beam velocity in many cases is only a weak function of distance, the corkscrew may be wound with constant pitch rather than with the tapered pitch that is called for by Eq. (3). For example, a total change in axial kinetic energy of about 10 percent corresponds to a change of only 5 percent in velocity over the total length of the corkscrew. For a 3-4 turn corkscrew, the required tapering would call for a winding accuracy beyond the mechanical tolerance limits within which each turn can be placed. However, one must realize that a nonideal corkscrew (i.e., one with fringing end fields and with imprecisely spaced turns) is bound to degrade even an incoming mono-energetic beam so that some velocity spread will appear at the corkscrew exit. Similarly, a moderate spread in the velocity of the incoming beam is, in effect, amplified during passage through the corkscrew region. Analytical expressions for the geometry of an optimally efficient corkscrew, and the current required to produce a given energy conversion with a given beam, are available (ref. 19). The required calculations are laborious, but a computer program has been written and the results have been verified experimentally with great accuracy.* As the corkscrew current usually can be adjusted over some range, the following rough approximation may be used if the desired transverse field is known. The bifilar helix is modeled by a series of interleaved planar current loops (Figure 2). The axial field components cancel, and the transverse field becomes that of two straight parallel wires spaced a distance $2 r_c$ apart. On the beam axis, one then finds for the transverse field strength

$$B_{\perp} \approx \mu_0 I / \pi r_c . \quad (4)$$

*W. Getty, University of Michigan, to be published.

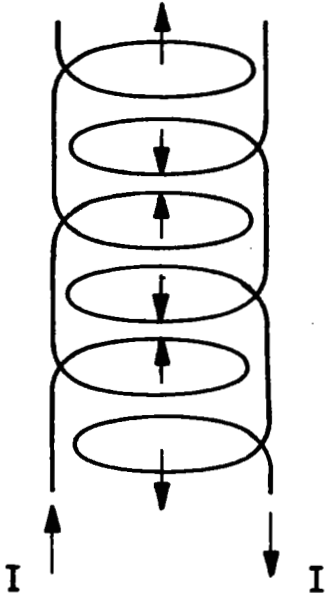


Figure 2.- Approximation used for calculating the transverse magnetic field of a bifilar helix.

For example, on a corkscrew with a 2-cm mean diameter and a 10-cm pitch, Eq. (4) was found to predict the measured field perturbation (0.43 Gauss per Ampere) within better than ten per cent.

The radial decay of the transverse magnetic field perturbation away from the corkscrew has a modified Bessel function dependence (ref. 18).

$$f(r) \sim I_0 \left(\frac{2\pi r}{p_c} \right) - \frac{p_c}{2\pi r} I_1 \left(\frac{2\pi r}{p_c} \right) \quad (5)$$

In order to make $f(r) \approx$ constant over the beam cross-section, it is clearly desirable to make the corkscrew pitch p_c and hence also, the beam velocity u large.

One might note here that immersed flow implies essentially a slipping-stream beam, in which the axial velocities are non-uniform over the beam cross section, in contrast to a Brillouin beam. Consequently, the synchronism condition Eq. (3) cannot be met by all electrons simultaneously, so that the inherent velocity spread on the incoming beam will, in fact, be amplified by the corkscrew action. To avoid this, one clearly should either use Brillouin flow or else resort to a very thin beam.

In addition to the magnetic corkscrew, other methods of shaping the initial beam trajectory are possible, such as

electrostatic corkscrews or deflection plates, and various ways of injecting the electrons at an angle to the magnetic field lines. Strictly as a laboratory device, the simple magnetic corkscrew seems to perform rather well, however.

Once started on their spiraling trajectory, the electrons are allowed to drift into a region of increasing magnetic field B_1 , here called a mirror region. It is assumed that the change in field is slow enough so that the electrons will not cross flux lines, and the magnetic moment will thus be conserved (the adiabatic assumption). Then it can be shown (ref. 20) that, as B_1 increases, the orbits decrease in size and also move closer together, each guiding center remaining on a flux line and each orbit within a tube of flux. The kinetic energy of the circular motion will increase directly proportional to the magnetic field strength, at the expense of the axial energy (see Figure 3),

$$\text{magnetic moment} \triangleq \frac{1}{2} \frac{mw^2}{B_1} = \text{constant} . \quad (6)$$

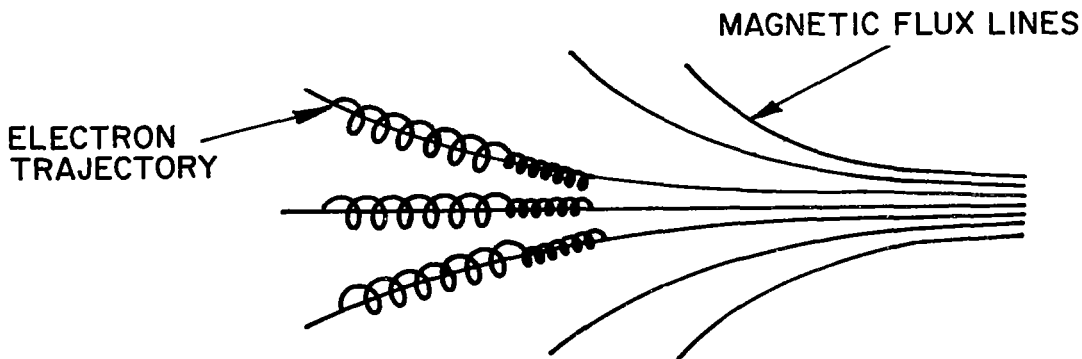
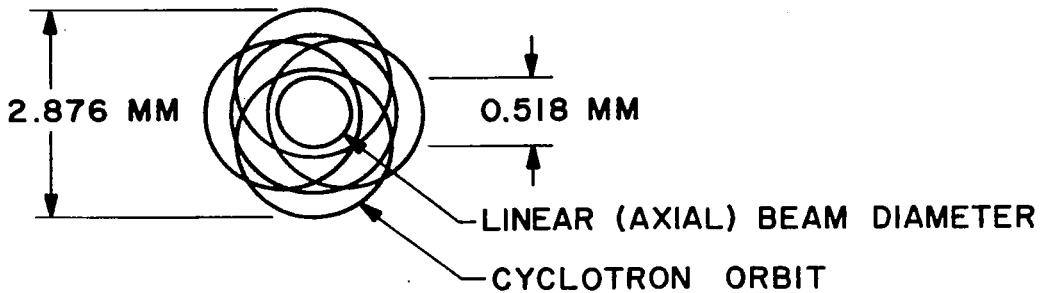


Figure 3.- Magnetic compression of a beam of spiraling electrons, assuming the compression to be adiabatic.

A typical beam cross-section such as might result with a 15-keV beam after nearly 100 percent conversion of axial energy, orbiting in a 3500-G magnetic field, is shown in Figure 4. Throughout this discussion, the assumption is being made that the electrons are spiraling individually, each about its own guiding center. While this assumption is certainly true of a linear, confined-flow beam, direct experimental observation of

A) ELECTRONS SPIRALING INDIVIDUALLY



B) ELECTRONS SPIRALING COLLECTIVELY

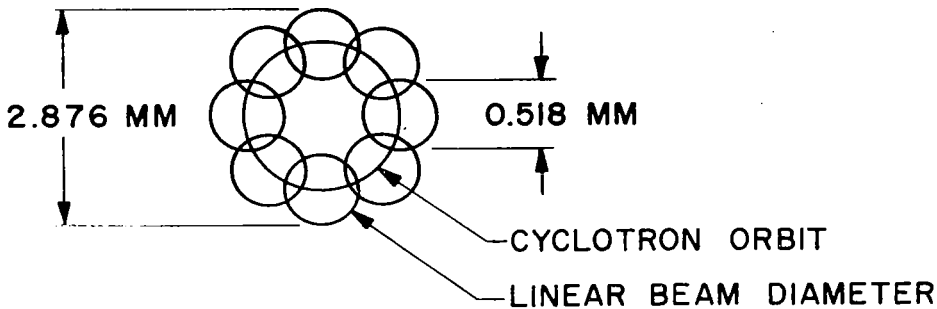


Figure 4.- Cross-section of 15 keV beam of spiraling electrons after nearly 100 percent energy conversion.

spiraling beams has shown that under the influence of the corkscrew perturbation, the beam as a whole will assume a helical shape, fixed in space. However, after passage into the mirror field, with nearly 100 percent of the axial kinetic energy converted, the pitch of the helical electron orbits will approach zero in either case, and the outer diameter of the resulting rotating electron cloud will ideally be the sum of the original beam diameter and the orbit diameter. An experiment was carried out in which the beam was allowed to impinge on a tungsten-mesh target, exciting the latter to local incandescence. The incandescent outline of the beam was viewed through a glass window while the pitch of the electron orbits was gradually decreased by increasing the corkscrew current. The fact that the beam outline then was seen to bloom out symmetrically from the center, without any observable lateral movement across the target, clearly favors the picture of electrons spiraling individually at this point.

Actually, with the zero-space-charge conditions assumed in the small signal kinetic theory below, the distinction between individual and collective spiraling is unimportant, because the

electrons then act in any case as independent, identically phased sources driving the cavity (ref. 7). In this report, for simplicity, individual spiraling of the electrons will be assumed.

With this assumption, one can calculate the beam diameter as a function of the axial magnetic field strength. The initial linear beam diameter d_0 will undergo magnetic compression,

$$d_1 = d_0 \sqrt{\frac{B_0}{B_1}} \quad (7)$$

where B_0 = magnetic field linking the cathode, and d_1 = linear beam diameter at some distance along the axis, with $B = B_1$. Using the data in Figure 4, one superimposes the cyclotron orbits of the individual electrons on the compressed linear diameter, in such a way that each electron retains its original guiding center. The resultant overall beam diameter then becomes

$$D = d_1 + 2r_b \quad (8)$$

where r_b = cyclotron radius. A plot of D versus axial distance is shown in Figure 5, for the device described in Figure 1. A beam of 15-keV electrons that initially has a 2-mm diameter, first expands while passing through the corkscrew and then contracts under the influence of the increasing axial magnetic field, reaching a final diameter of 3 mm at $B = 3.43$ kG (cyclotron frequency 9.6 GHz), with all its kinetic energy in the transverse direction. Note that the beam diameter shown in the corkscrew region is only approximate.

We now return to the problem of velocity spread. As mentioned before, winding irregularities and the transverse field variation on the corkscrew are apt to generate some velocity spread on an initially mono-energetic beam, or will increase whatever velocity spread already exists on the beam. In addition, the action of the mirror field will itself be such as to increase the relative width of any velocity spread. The conversion of axial to transverse energy in effect moves the initial distribution which may have been, for example, a narrow Gaussian centered about 15 keV, closer to the origin, and the distribution may be truncated or otherwise distorted as the slowest electrons begin to be turned around by the magnetic mirror. Also, space charge effects will begin to be important as the beam is slowed axially, and this will result in potential depression near the beam center, and will thus increase the velocity spread.

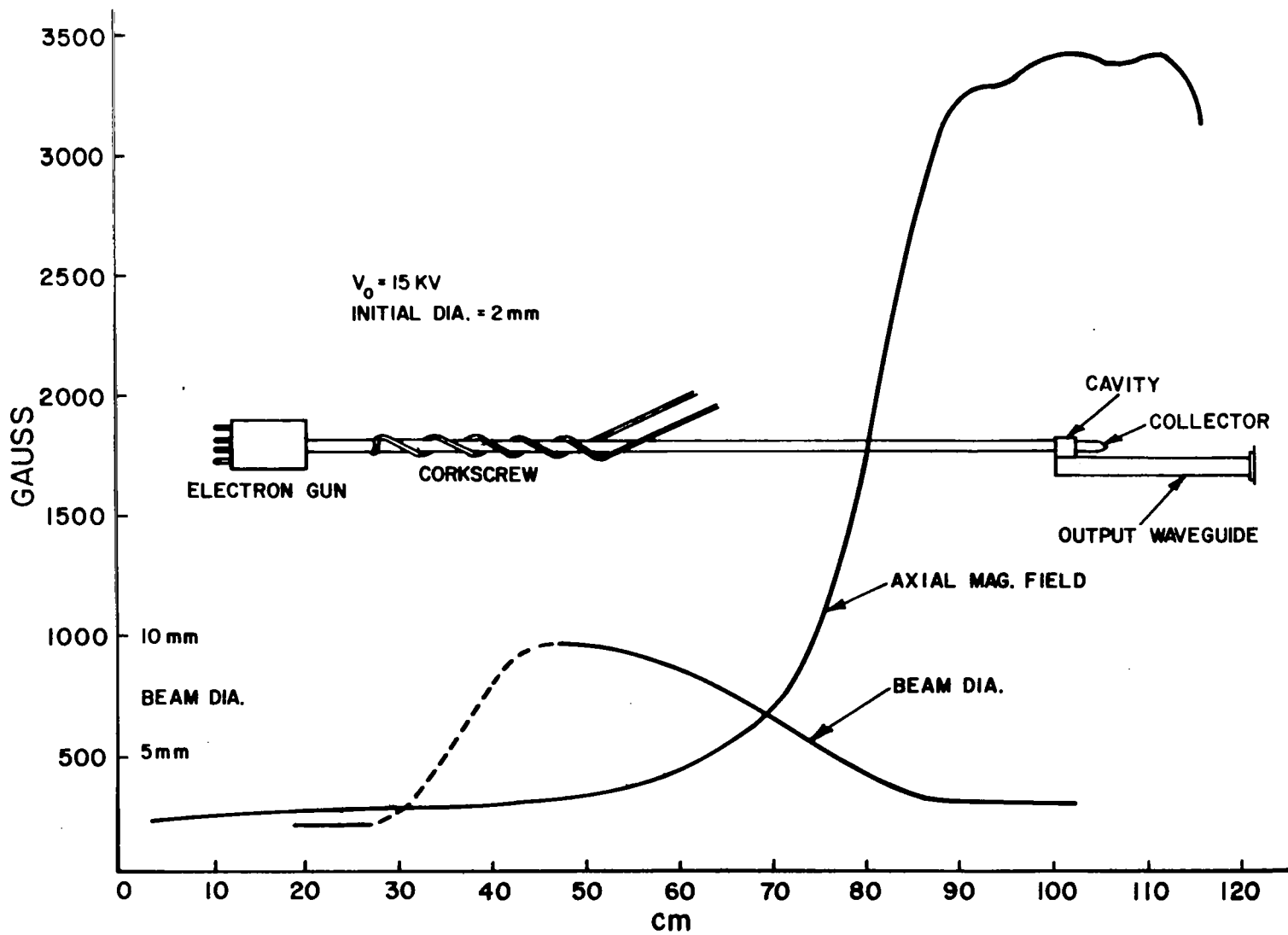


Figure 5.- Calculated beam profile, shown to scale with axial magnetic field.

One should note that these effects all arise even with a mirror field that completely satisfies the adiabatic assumption, i.e., where the spatial rate of change of magnetic field is very gradual. "Gradual" has been described by Allis (ref. 20) with the inequality

$$|\vec{\nabla}B_1| \ll \frac{B_1}{r_b} \quad (9)$$

which means, essentially, that any spatial change in B_1 should be distributed over a distance large compared to the cyclotron radius. For example, at the steepest point of the field profile shown in Figure 1, the characteristic distance is

$$\frac{B}{\text{grad } B} = 90 \text{ mm} ,$$

and this is far greater than the cyclotron radius at that point, $r_b = 1.64 \text{ mm}$.

If the adiabatic assumption is not satisfied, then the electrons will begin to cross flux lines, and this will further increase the velocity spread. As an air-core solenoid system will generally result in smaller field gradients than one where iron pole pieces are used, the former is preferable and thus has been used with the in-house X-band device. For devices that employ superconducting magnets, pole pieces would saturate and thus are not used in any case.

A word should be added here about standing-wave (resonant) versus traveling-wave (backward-wave) interaction with the spiraling beam. It has been mentioned that the resonant interaction is more economical in terms of the required volume of uniform magnetic field. However, the existence of velocity spread on the beam probably favors axially long interaction regions, because these, together with some inevitable magnetic field non-uniformities, may well serve to utilize a greater velocity range of electrons for the interaction. This may in fact be the reason why the devices using backward-wave interaction have generally been found to be more efficient than standing-wave devices. More definite information should become available once a planned numerical large-signal analysis has been completed.

One more question which must here be left unanswered, is how much of the conversion of axial to transverse energy should be accomplished by the corkscrew, and how much by the magnetic mirror. Resolution of this problem will become clearer once

more is known about the way in which corkscrew and mirror fields operate on the velocity distribution.

START-OSCILLATION CURRENT FOR A MONO-ENERGETIC BEAM

In this section, the small-signal theory will be summarized. The electron beam inside the cavity is considered as a cloud of slowly drifting electrons, each orbiting at the cyclotron frequency about a magnetic flux line. The inclusion in the theory of an arbitrary velocity distribution in principle allows one to take into account varying degrees of velocity spread. The electron cloud is assumed to be made macroscopically neutral by the presence of immobile ions, and is assumed to be sufficiently tenuous such that electron-ion collisions and electron-electron collisions (rf space-charge effects) can also be neglected. Given the original electron velocity distribution, the linearized Boltzmann-Vlasov equation is solved for the perturbed (i.e., ac) part of the distribution function in terms of the known electromagnetic field components within the cavity. The ac density follows by integrating over the electron velocity distribution, and the power flow from the electrons to the rf cavity fields is derived by integrating the $\vec{J} \cdot \vec{E}$ product over the cavity volume. (It is assumed that the cavity modes are only insignificantly perturbed by the presence of the free charges.) The result is, after some manipulation,

$$P = - \frac{\pi}{2} \frac{e^2 E^2}{m k_{\parallel}^2} \rho(k_{\perp} a) \int dw \int du f_0(u, w) \frac{w}{u} G_{\omega}(x) [1 + \beta Q_{\omega}(x)] \quad (10)$$

This equation describes the following situation. The column of electrons, with radius "a," drifts axially through the cavity, with the rf electric field polarized at right angles to the beam. The electrons initially have a velocity distribution $f_0(u, w)$, where u and w are the axial and transverse velocity components, respectively. The term $\rho(k_{\perp} a)$ represents the number of electrons per unit length of the beam, weighted by the variation of the rf electric field over the beam cross-section, and $G_{\omega}(x) [1 + \beta Q_{\omega}(x)]$ is the so-called gain function, which describes the dependence of the absorption behavior on the transit time and on the synchronism conditions of the beam electrons. The remaining symbols have their usual meaning,

e, m = electronic charge, mass

k_{\parallel}, k_{\perp} = axial and transverse components of the wave vector k

E = amplitude of the rf electric field vector interacting with the beam.

In order to derive a simple approximate expression for the start-oscillation current, the following restrictions are now placed on Eq. (10). First, we assume a mono-energetic beam,

$$f_0(u, w) = \frac{1}{2\pi w_0} \delta(u - u_0) \delta(w - w_0) . \quad (11)$$

The second assumption concerns $\rho(k_{\perp} a)$. For the referenced experiment (ref. 7), a 3-mm diameter, spiraling beam traverses a rectangular TE_{101} cavity ($f = 9.463$ GHz), of length $L = 2.14$ cm and cross-section 2.29×1.02 cm, at right angles to the electric field vector, and the electric field variation over the beam cross section is very small. Hence, one may approximate $\rho(k_{\perp} a)$ by a constant

$$\rho_0 \approx \frac{I_0}{u_0 e} \quad (12)$$

where $I_0 =$ dc beam current. Substituting Eqs. (11) and (12) into (10),

$$P = \frac{e E^2}{4mk^2} \cdot \frac{I_0}{u_0^2} \cdot G_{\omega} (1 + \beta Q_{\omega}) . \quad (13)$$

For oscillations to start, the power extracted from the beam is just balanced by the losses in the cavity walls plus the external load,

$$P_{\text{loss}} = \frac{\omega U}{Q_L} \quad (14)$$

where $U =$ stored energy and Q_L has its usual meaning. Finally, equating Eqs. (13) and (14), one finds the start-oscillation current

$$I_{\text{start}} = \frac{4\pi^2}{\eta\tau^2} \cdot \frac{\omega U}{Q_L E^2} \cdot \frac{1}{G_{\omega} (1 + \beta Q_{\omega})} \quad (15)$$

where $\tau = L/u_0$ denotes the transit time through the cavity, and $k_{\parallel} = \pi/L$ was used, corresponding to the TE_{101} resonance in a cavity of length $L = 2.14$ cm.

As will be shown, Eq. (15) leads to results that are in reasonably close agreement with experimental data. Its real significance, however, is that it points out those physical parameters which bear on the small-signal electronic gain of the device and which probably also have some influence on the saturated power output and the efficiency. These factors will now be considered in greater detail.

CAVITY LOADING AND GEOMETRY

The inverse dependence of I_{start} on Q_L was well confirmed through measurements (ref. 7) where Q_L was varied by changing the external loading, with

$$\frac{1}{Q_L} \equiv \frac{1}{Q_0} + \frac{1}{Q_{\text{ext}}} . \quad (16)$$

For convenience, these results are reproduced in Figure 6.

It is illuminating to consider a simple model where the presence of the beam causes a negative conductance G_e to appear in parallel with the cavity shunt conductance G_{sh} , and the start-oscillation condition corresponds to $|G_e| \geq G_{\text{sh}}$. As one can write

$$\frac{1}{Q_L} = \frac{R_{\text{sh}}}{Q_0} \cdot \frac{Q_0}{Q_L} \cdot G_{\text{sh}} , \quad (17)$$

where the first two terms depend only on the geometry of the cavity and the coupling iris respectively, it is clear that

$$G_{\text{sh}} \sim \frac{1}{Q_L} \quad (18)$$

and hence,

$$|G_e| \sim \frac{1}{Q_L} \sim I_{\text{beam}} \quad (19)$$

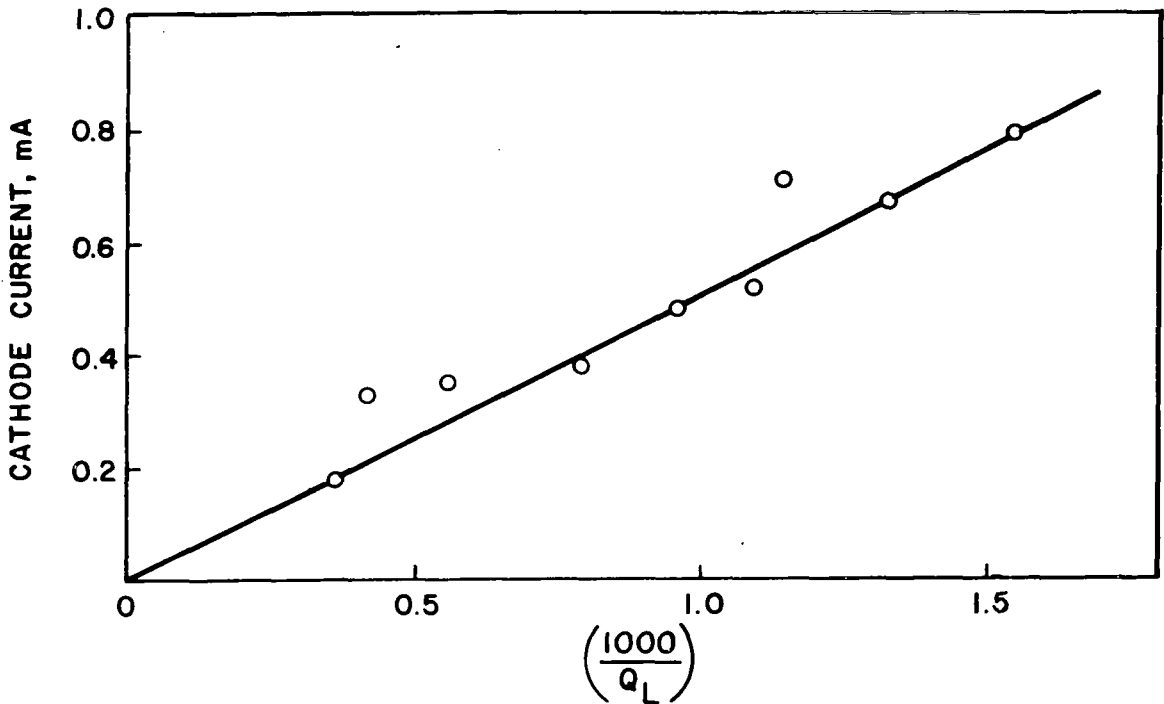


Figure 6.- Start-oscillation current versus $1/Q_L$, for the device shown in Figure 1.

at start-oscillation. One concludes that in the small-signal regime, the negative beam-loading conductance G_e is directly proportional to the beam current, that is, the orbiting electrons act as a linear superposition of individual, identically phased sources driving the cavity fields. This agrees with the zero-space-charge assumption made earlier.

In Eq. (15), the influence on I_{start} of the cavity geometry is described by the factor $E^2/\omega U$. For want of a better term, this factor will be called the "shape parameter" of the cavity, because it provides a measure of the effectiveness of a given amount of rf stored energy, U , in setting up the interaction field intensity, E . Clearly, if a small I_{start} is desired, the cavity should be designed in such a way that most of the electric energy is stored in the region traversed by the beam.

The similarity of the "shape parameter" to the normalized shunt impedance of the cavity is evident,

$$\frac{R_{sh}}{Q_0} \equiv \frac{V^2}{2\omega U} , \quad (20)$$

where V stands for the peak value of the rf voltage drop experienced by an electron in transit through the cavity; i.e., the line integral of the rf electric field vector along the path of the electron. It is patently difficult to write such an integral for an electron orbiting in the electric field, especially since the number of orbits is not easily determined. However, for many practical cavities one may assume a reasonably constant electric field in the interaction space, and then arbitrarily let

$$V \approx E_0 b \quad (21)$$

where b = gap spacing, determined mainly by the required beam clearance. With this assumption one then finds

$$\frac{E^2}{\omega U} = \frac{2}{b^2} \cdot \frac{R_{sh}}{Q_0} \quad (22)$$

An approximate calculation of the beam diameter has already been carried out and is shown in Figure 5.

Inside the cavity, the beam diameter is expected to be about 3 mm, however, a larger gap spacing (7.62 mm) was assumed arbitrarily to make allowance for some error in beam alignment. Figure 7 shows the calculated values of the "shape parameter" for some simple cavity geometries. All the applicable cavity dimensions are optimized to give maximum $E^2/\omega U$ at $f_0 = 9.6$ GHz, with the beam clearance as stated above.

It is seen that the cylindrical TM_{010} and the rectangular TE_{101} cavities have almost identical shape parameters. However, the latter has slightly smaller internal losses (greater Q_0) and also is fitted more easily to a rectangular feeder waveguide. Hence, for operation at 9.6 GHz, the rectangular cavity is the best of the simple shapes; further improvement may be possible by going to more complex, empirical designs, e.g., by adding a center post to the cavity.

A similar calculation may be made at 94 GHz. Assuming the same initial beam diameter, the final diameter will be 0.442 mm in an axial field of 33.6 kG, corresponding to a 94-GHz cyclotron frequency. This beam fits easily through a rectangular TE_{101} cavity consisting of a resonated section of WR-10 guide, with cross-section of 2.54×1.27 mm.

At higher frequencies, the internal cavity losses will dissipate an increasing proportion of the total rf power extracted

| Field Configuration | Description | $E_m^2/\omega U$ |
|---------------------|--|--|
| | Rectangular TE_{101} (Square Base) | 4.04×10^6 ohms/m ² $Q_o = 8400$ |
| | Cylindrical TM_{010} | 4.08×10^6 ohms/m ² $Q_o = 6900$ |
| | Cylindrical TE_{111} (Min. beam clearance does not apply) | 1.56×10^6 ohms/m ² |
| | Cylindrical TE_{011} (Min. beam clearance does not apply) | 0.34×10^6 ohms/m ² |
| | Spherical biconical, order of resonance $n = 3$ | 3.04×10^6 ohms/m ² |

Figure 7.- Shape parameter for some simple cavity geometries, optimized at $f = 9.6$ GHz. The beam path is indicated by the dotted arrows; the electric field lines by the solid arrows.

from the beam. For example, the theoretical Q_0 for a rectangular TE_{101} cavity is 7800 at 9.6 GHz, and drops to 2800 at 94 GHz, varying roughly as $(f)^{-1/2}$. The choice of a larger volume-to-surface ratio will increase Q_0 , as for example a spherical biconical cavity, heavily overmoded, can easily produce a Q_0 greater than 10,000 at X-band (ref. 21). However, Q_0 is then traded off against the shape parameter because in the overmoded cavity most of the electromagnetic energy will be stored away from the interaction region. The same comment can be made about quasi-optical (overmoded) resonators in general, including Fabry-Perot etalons.

On the other hand, one application where small cavities have been used successfully even up to 700 GHz is that of frequency-multiplier klystrons (ref. 22), and this is one example which illustrates a design for maximum cavity impedance (shape parameter) even at a sacrifice in Q_0 .

THE GAIN FUNCTION

The gain function $G_\omega(x) [1 + \beta Q_\omega(x)]$ summarizes the basic mechanism by which electrons orbiting through the cavity at the proper velocity, will drift into an accelerating or a retarding phase and hence, will absorb energy or give up energy to the cavity fields.

A good physical description of the relativistic bunching mechanism, which dominates the interaction with a standing wave, has been given by Hsu (ref. 16). The key to this mechanism lies in the fact that any change in the kinetic energy of the orbiting electrons as they interact with the transverse electric field of the cavity, will primarily affect the radius of gyration. The gyrofrequency is affected only slightly through the relativistic velocity dependence of the electron mass, and it is this slight change which can produce the desired bunching.

The process can be illustrated by considering three electrons which enter the interaction region with the rotating electric field vector in a decelerating (decel), neutral, and accelerating (accel) phase, respectively. The linearly polarized cavity field is here represented by two counter-rotating, circularly polarized vector components, only one of which will interact with the orbiting electrons. It is assumed that the gyrofrequency of the entering electrons is set lower than the field frequency. Thus the first electron, which enters in the decel phase, would normally lag behind the rotating field vector and would eventually fall into the accel phase. However, as the electron loses kinetic energy, this phase slippage is partially cancelled by the relativistic decrease in mass and the consequent increase in

gyrofrequency, i.e., this electron tends to be "held" in the decel phase.

On the other hand, the second electron which is initially in the neutral phase, will simply slip into the decel phase. Similarly, the third electron, initially in the accel phase, will gain in mass, decrease its gyrofrequency, and will quickly also slip into the decel phase. The result is the desired bunching of electrons in the decel phase, i.e., a transfer of energy from the electrons to the cavity fields, or a net emission of microwave power. By similar reasoning, it is easy to show that if the gyrofrequency is set higher than the field frequency, net power absorption will result. Over a narrow range of gyrofrequency, then, the rotating electron cloud will go from a peak of positive to one of negative absorption, and this behavior has been verified experimentally (ref. 2).

The gain function depends on the two variables:

$$x = \frac{\Omega - \omega}{k_{\parallel} u_0} = \frac{\Omega - \omega}{\pi} \tau \quad (23)$$

where $\Omega = (e/m)B_1$ is the (relativistic) cyclotron frequency, and

$$\beta = \frac{k_{\parallel} w_0^2}{\omega u_0} = \frac{\pi w_0^2 \tau}{\omega_L^2} \quad (24)$$

A mono-energetic beam is assumed, with $u = u_0$ and $w = w_0$. In effect, x describes the total phase lead or lag accumulated by an electron in passing through the cavity, referred to the phase of the rf electric field vector, whereas β is a measure of the (transverse) beam energy and of the transit time.

A plot of $G_{\omega}(x) [1 + \beta Q_{\omega}(x)]$, with

$$G_{\omega}(x) = \frac{\cos^2\left(\frac{\pi x}{2}\right)}{(1 - x^2)^2} \quad (25)$$

and

$$Q_{\omega}(x) = x - \frac{1}{2G_{\omega}} \frac{dG_{\omega}}{dx} \left[\frac{\omega^2}{k_{\parallel}^2 c^2} - x^2 \right] \quad (26)$$

is given in Figure 8, as calculated for the rectangular TE₁₀₁ cavity (ref. 7). For each value of β , there is a value of x (generally, $x \approx -0.85$) that will result in maximum negative absorption (beam loading), and the amount of negative absorption increases as β is increased. Clearly, $x \approx -0.85$ is easily achieved by adjusting the magnetic field strength, but once more the maximum value of β is limited, for a given beam energy, by the physically realizable value of the transit time. A sharply peaked velocity distribution, therefore, emerges forcefully as an important design goal.

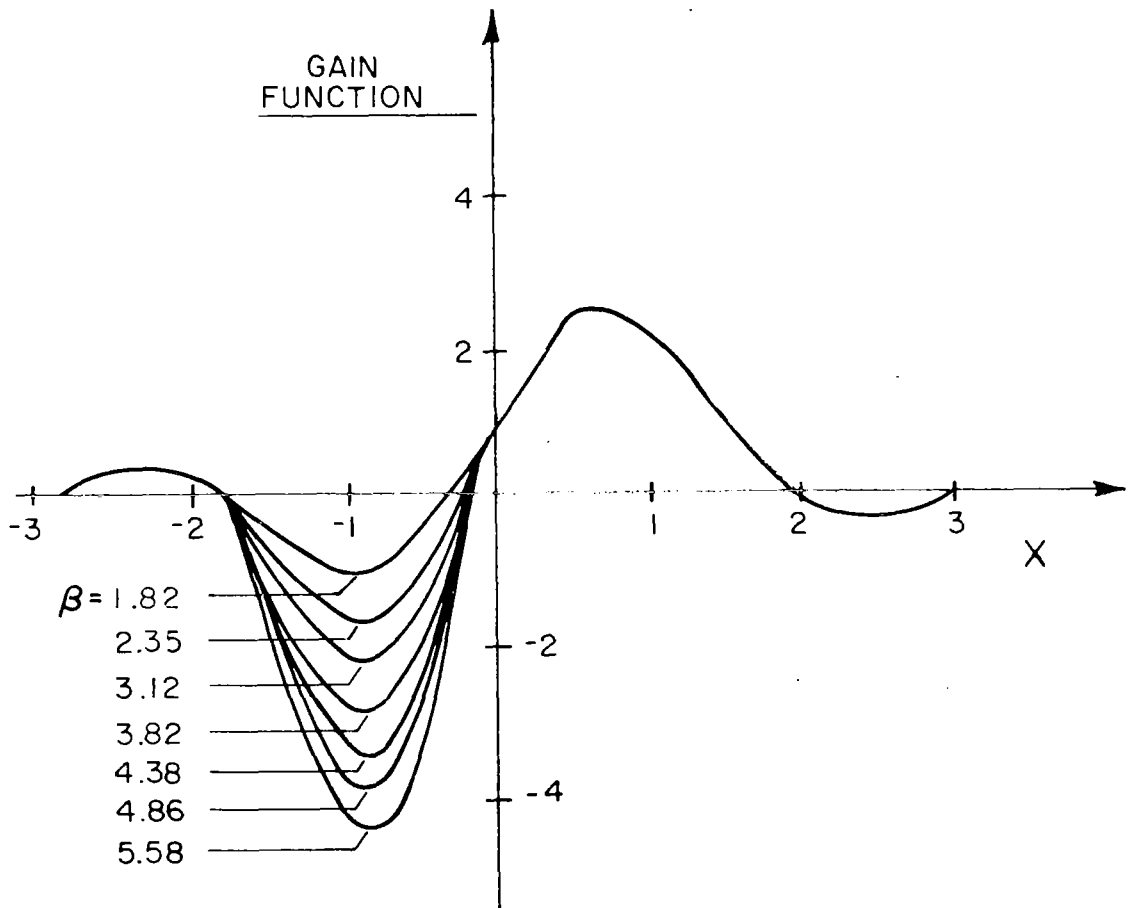


Figure 8.- Gain function versus x , for the device shown in Figure 1. The parameter is β .

The inverse dependence of I_{start} on the square of the transit time in effect defines an ideal condition where there is just a rotating electron cloud inside the cavity, with zero axial motion and, hence, infinite transit time. This condition cannot be reached in practice, of course, because of space-charge limitations, and because of the inevitable velocity spread on the beam, i.e., the slowest electrons will be turned around by the magnetic ramp (ref. 3), the fastest electrons will be out of synchronism, and only the electrons corresponding to the central part of the velocity distribution will actually be available for interaction with the cavity fields.

A precise experimental check of the theoretical prediction of I_{start} is quite impossible until something about the actual velocity distribution of the beam and, hence, an average transit time, is known. One way to measure the velocity distribution is by means of a retarding-field analyzer. However, special care must be taken to allow for the non-rectilinear trajectory of the beam electrons (ref. 23).

A rough estimate of the transit time for electrons near the peak of the velocity distribution can be had by resorting to the gain characteristic. Clearly, oscillations generally will occur when the negative beam loading is maximum, so the slip parameter will have a value $x = (\Omega - \omega/k_{\parallel}u) \approx -0.85$, and with $\Omega = (e/m)B$, ω , and k_{\parallel} all known, this determines u_0 and, hence, the transit time. For example, with a 15-keV beam orbiting through a TE₁₀₁ cavity resonant at 9.6 GHz, the axial energy for peak negative beam loading is 84 V, corresponding to a transit time of 4 nsec through the 21 mm cavity length. The kinetic energy thus is almost entirely transverse, and the relativistic mass change of the electrons is 2.93%. The value of B_1 measured was 3439 ± 10 Gauss, and this corresponds to a relativistic cyclotron frequency that is 1.2 percent below the cavity oscillation frequency of 9.463 GHz.

One may go on to calculate the start-oscillation current as follows. The parameter

$$\beta = \frac{k_{\parallel}}{\omega} \frac{w_0^2}{u_0} = 2.29$$

and with this one enters the graph of gain function vs. slip parameter (Figure 8); this gives $G_{\omega}(1 + \beta Q_{\omega}) = -1.6$. The shape parameter $E/\omega U = 3.06 \times 10^6$ ohms/m² for this cavity. Finally, from Eq. (15) one gets

$$I_{\text{start}} Q_L = 75.3 \text{ mA (calculated).}$$

In comparing this value to the experimental result, one can, at best, bracket the "true" beam current within a maximum (the measured cathode current) and a minimum (the measured collector current). From reference 7, where the cathode current is used,

$$I_{\text{start}}^{Q_L} = 515 \text{ mA (measured),}$$

whereas, if the collector current were used,

$$I_{\text{start}}^{Q_L} = 129 \text{ mA (measured).}$$

In either case, the agreement is better than order-of-magnitude. The main source of error in the theory probably is in the assumption of a delta-function velocity distribution (zero velocity spread).

CALCULATION OF EFFICIENCY

The analysis of the previous sections was based on an expression for start-oscillation current that itself was derived from a linearized theory, with the assumption of a mono-energetic beam. The start-oscillation current probably is a reasonably good qualitative predictor of efficiency, in that it gives an indication of the intensity of the beam-cavity interaction. However, as with any oscillator, the steady-state amplitude of the output is determined by non-linear, large signal phenomena, which call for entirely different computational procedures. Hsu (ref. 16) has formulated an analytical but very unwieldy expression for the efficiency, based on including both first- and second-order terms in an assumed series solution to the Lorentz equation. However, in view of this early truncation of the series solution, it seems doubtful whether the resulting expression is really valid for large-signal conditions, and one is hardly tempted to go through the complex calculations necessary to derive a numerical result from Hsu's formulas. The Russian literature (refs. 4 and 6) gives estimates of the theoretical efficiency as high as 24 percent; however, as no derivations of their formulas are given, these estimates are difficult to accept without some skepticism. Thus, despite the obvious computational difficulties, a reliable estimate of the theoretical efficiency is probably best obtained by direct numerical integration of the electronic equations of motion for a specific set of assumed conditions.

For completeness, Figure 9 summarizes the measured limiting-amplitude (saturated) behavior of the device shown in Figure 1, giving power output and efficiency in terms of the cathode current. The beam transmission to the collector was typically near 25 percent, and a less conservative estimate of the efficiency, defined in terms of the minimum current known to be available for interaction with the cavity, would therefore be close to four percent at the maximum.

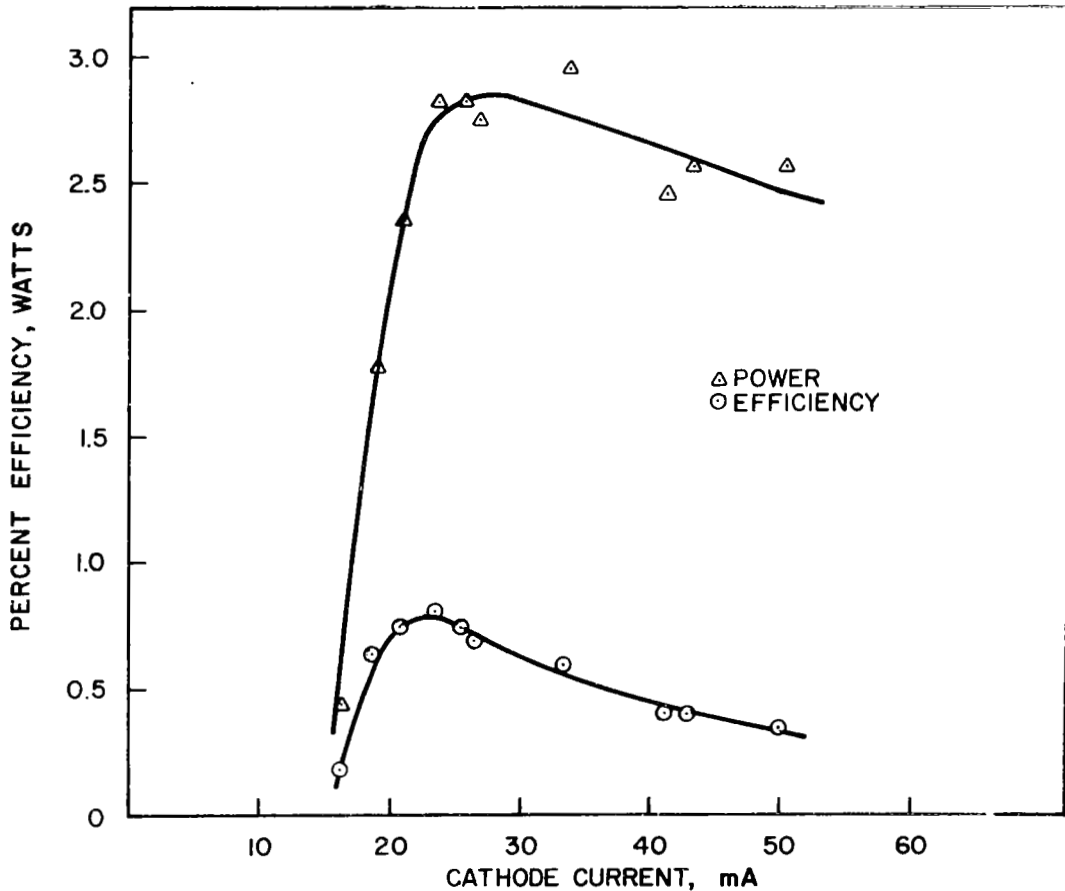


Figure 9.- Power output and efficiency versus beam current for the device shown in Figure 1.

A phenomenon which seems at first to be a serious limitation on the power output of cyclotron resonance oscillators, is the so-called cyclotron resonance breakdown (see Appendix B). Fortunately, the margin between breakdown conditions and operating conditions can be made adequately wide, especially with high-velocity beams.

CONCLUSIONS

In the foregoing, results derived from the small-signal kinetic theory, together with some experimental data, have been used to bring out those physical parameters that dominate the electronic gain of cyclotron resonance devices. These are, the cavity geometry, the loaded Q , the transit time, and the single-electron gain function. The latter, in turn, is a function of the transverse kinetic energy, the synchronism conditions, and the transit time. A very long transit time is desirable, but is physically realizable only with a sharply peaked electron velocity distribution, and to achieve the latter, therefore, is an important design goal. A numerical example is given to indicate that the start-oscillation current can be predicted within a factor of 2-5 even with strong simplifying assumptions.

Electronics Research Center
National Aeronautics and Space Administration
Cambridge, Massachusetts, January 1969
109-02-03-01

REFERENCES

1. Bott, I. B.: A Powerful Source of Millimeter Wavelength Electromagnetic Radiation. Phys. Letters, vol. 14, February 1965, pp. 293-294.
2. Hirshfield, J. L., Bernstein, I. B., and Wachtel, J. M.: Cyclotron Resonance Interaction of Microwaves with Energetic Electrons. IEEE J. Quantum Electronics, vol. QE-1, September 1965, pp. 237-245.
3. Schriever, R. L., and Johnson, C. C.: A Rotating Beam Waveguide Oscillator. Proc. IEEE, vol. 54, 1966, pp. 2029-2030.
4. Gaponov, A. V., et al.: Induced Synchrotron Radiation of Electrons in Cavity Resonators. JETP Letters, vol. 2, November 1, 1965, pp. 267-269.
5. Beck, A. H., Edgcombe, C. J., and Kenyon, N. D.: A Microwave Device Incorporating Adiabatic Compression of a Rotating Annular Beam. Proc. 6th Int. Conf. Microwave and Optical Generation and Amplification, Cambridge, Sept. 1966. IEE Conf. Publ. 27, The Institution of Electrical Engineers, Savoy Place, London WC 2, England, pp. 191-197.
6. Antakov, I. I., Gaponov, A. V., Malygin, O. V., and Flyagin, V. A.: Application of Induced Cyclotron Radiation of Electrons for the Generation and Amplification of High-Powered Electromagnetic Waves. Radio Engr. and Elect. Phys., vol. 11, 1966, pp. 1995-1998.
7. Kulke, B., and Wilmarth, R. W.: Small-Signal and Saturation Characteristics of an X-band Cyclotron-Resonance Maser. Proc. IEEE, (letters), vol. 57, February 1969.
8. Pierce, J. R.: Traveling-Wave Tubes. Van Nostrand, New York, 1950.
9. Chow, K. K., and Pantell, R. H.: A Small-Signal Analysis of the Electron Cyclotron Backward-Wave Oscillator. Trans. IEEE, vol. ED-9, July 1962, pp. 351-358.
10. Sehn, G. J.: Relativistic Interaction between a Slow, Rotating Electron Beam and a Microwave Field inside a Waveguide at the Cyclotron Frequency. Doctoral Thesis, Dept. of Electrical Engineering, University of Colorado, Boulder, CO., September 1967.

11. Schriever, R. L., Durney, C. H., Johnson, C. C., and Grow, R. W.: Transverse-Wave Interactions between Rotating Electron Beams and Waveguides, Technical Report. Dept. of Electrical Engineering, University of Utah, Salt Lake City, Utah, April 1968.
12. Pierce, J. R.: Coupling of Modes of Propagation. J. Appl. Phys., vol. 25, February 1954, pp. 179-183.
13. Siegman, A. E.: The Waves on a Filamentary Electron Beam in a Transverse-Field Slow-Wave Circuit. J. Appl. Phys., vol. 31, January 1960, pp. 17-26.
14. McIsaac, P. R.: Research into Advanced Concepts of Microwave Power Amplification and Generation Utilizing Linear Beam Devices. Semiannual Status Report No. 2, School of Electrical Engineering, Cornell University, NASA Research Grant NGL-33-010-047, July 1968.
15. Hsu, T. W., and Robson, P. N.: Negative Absorption from Weakly Relativistic Electrons Traversing a Cuccia Coupler. Electronics Letters, vol. 1, no. 4, June 1965, pp. 84-85.
16. Hsu, T. W.: Coherent Millimetre-Wave Cyclotron Radiation from Relativistic Electrons. Doctoral Thesis, Dept. of Electronic and Electrical Engineering, University of Sheffield, Sheffield, England, August 1966.
17. Jory, H.: Investigation of Electronic Interaction with Optical Resonators for Microwave Generation and Amplification. Final Report, ECOM-01873-F, Varian Associates, Palo Alto, Calif., July 1968.
18. Wingerson, R.: Corkscrew - A Device for Changing the Magnetic Moment of Charged Particles in a Magnetic Field. Phys. Rev. Letters, vol. 6, May 1, 1961, pp. 446-448.
19. Wingerson, R. C., Dupree, T. H., and Rose, D. J.: Trapping and Loss of Charged Particles in a Perturbed Magnetic Field. Physics of Fluids, vol. 7, no. 9, September 1964, pp. 1475-1484.
20. Allis, W. P.: Motion of Ions and Electrons. Handbuch der Physik, vol. 21, S. Flügge, ed., Springer-Verlag, Berlin, 1956, pp. 383-387.
21. Culshaw, W.: Resonators for Millimeter and Submillimeter Wavelengths. Trans. IRE, vol. MTT-9, March 1961, pp. 135-144.

22. Kuypers, W.: Experimental CW Klystron Multiplier for Sub-millimetre Waves. Proc. 6th Int. Conf., Microwave and Optical Generation and Amplification, IEE Conf. Publ. 27, The Institution of Electrical Engineers, Savoy Place, London, WC 2, England, September 1966, pp. 98-102.
23. Caulton, M.: Retarding-field Analyzers for the Measurement of Axial-velocity Distributions in Electron Beams. RCA Review, vol. 26, June 1965, pp. 217-241.
24. Panofsky, W. K. H., and Phillips, M.: Classical Electricity and Magnetism. 2nd ed., ch. 20, Addison-Wesley, 1962.
25. Schrader, W. J.: Some Non-linear Effects in Electron Cyclotron Resonance Discharges. Rijnhuizen Report 67-40, FOM-Instituut Noor Plasma-Fysica, Rijnhuizen, Jutphaas, Nederland, October 1967, MF Accession No. N68-25495.

APPENDIX A

SPONTANEOUS RADIATION

A well-known prediction of classical electromagnetic theory is that an accelerated charge will lose some of its kinetic energy by radiation (ref. A1). For a single electron orbiting with radian frequency Ω and tangential velocity $w \triangleq \beta c$, the radiated power is

$$P = \frac{e^2}{6\pi\epsilon_0 c} \Omega^2 \left(\frac{\beta^2}{1-\beta^2} \right) \text{ watts.}$$

If a large number of electrons are uniformly distributed in a circle spinning about its axis, the net radiation, however, will be zero. A uniform ring current does not radiate; some bunching around the circumference is necessary for net radiation to take place. If an ideal ensemble of identically phased orbiting electrons is assumed, one may linearly superimpose the radiated power contributions, and one may be tempted to use this as an estimate of the maximum conversion efficiency of a cyclotron resonance oscillator. It must be remembered, however, that such an estimate considers only the spontaneous cyclotron radiation and ignores the important $\vec{J} \cdot \vec{E}$ interaction with the cavity fields. Moreover, it is assumed that no energy is lost by radiation while the rotating electron cloud is being formed. Thus, the resulting expression probably has little validity in this case.

REFERENCES

- A1. Panofsky, W. K. H., and Phillips, M.: Classical Electricity and Magnetism. Second ed., Addison-Wesley Co., 1962, ch. 20.

APPENDIX B

CYCLOTRON RESONANCE BREAKDOWN

Cyclotron resonance breakdown at low pressure in an evacuated microwave cavity, as discussed recently by Schrader (ref. B1) has also been observed during our experiments (ref. B2). Typically, the cavity spontaneously changed its impedance to a milliwatt-level probing signal at the cavity resonant frequency as the ambient magnetic field was varied through cyclotron resonance. At pressures between 10^{-7} and 10^{-6} torr, breakdown typically occurred after a few microseconds. These results are in reasonable agreement with measurements by Schrader who found that the minimum power required for breakdown remains essentially constant at less than a milliwatt once the pressure is reduced below a certain minimum (in his case, 10^{-3} torr). He also found that the optimum magnetic field for breakdown is about 0.1 to 0.2 percent above the value corresponding to rest-mass cyclotron resonance, as compared to 0.2 percent to 0.6 percent observed by the author. Physically, cyclotron resonance breakdown apparently is caused by trapping of electrons in the rf fields within the cavity, so that locally the effective pressure is increased to the point where ordinary high-frequency breakdown would be expected. Evidently, a breakdown of this type could seriously interfere with the operation of a cyclotron resonance oscillator. Fortunately, with reasonably energetic electrons, the magnetic field required to produce the appropriate relativistic cyclotron frequency

$$\Omega = \frac{eB}{\gamma m_0} ,$$

where

$$\gamma = \left[1 - \left(\frac{w}{c} \right)^2 \right]^{-1/2} ,$$

is 1 to 2 percent above the value that would produce breakdown of the evacuated cavity. A semi-empirical relationship is

$$\frac{B(\text{start-osc.})}{B(\text{cyclo. br.})} \approx 0.99\gamma$$

and since this ratio should be made large, this is an argument in favor of high-velocity beams.

It is interesting to note that Antakov, et al. (ref. B3), also report cyclotron resonance breakdown in a traveling-wave device using a cycloidal sheet beam.

REFERENCES

- B1. Schrader, W. J.: Some Non-linear effects in Electron Cyclotron Resonance Discharges. Rijnhuizen Report 67-40, FOM-Instituut voor Plasma-Fysica, Rijnhuizen, Jutphaas, Nederland, MF Accession no. N68-25495, October 1967.
- B2. Kulke, B., and Wilmarth, R. W.: Small-Signal and Saturation Characteristics of an X-band Cyclotron-Resonance Maser. Proc. IEEE (letters), vol. 57, February 1969.
- B3. Antakov, I. I., Gaponov, A. V., Malygin, O. V., and Flyagin, V. A.: Application of Induced Cyclotron Radiation of Electrons for the Generation and Amplification of High-Powered Electromagnetic Waves. Radio Engr. and Elect. Phys., vol. II, 1966, pp. 1995-1998.

FIRST CLASS MAIL



POSTAGE AND FEES PAID
NATIONAL AERONAUTICS AND
SPACE ADMINISTRATION

69147 00903
C40 001 50 51 3DS
AIR FORCE WEAPONS LABORATORY/AFWL/
KIRTLAND AIR FORCE BASE, NEW MEXICO 87117

ATTN: E. LOU BOGART, ACTING CHIEF TECH. LIT

POSTMASTER: If Undeliverable (Section 158
Postal Manual) Do Not Return

"The aeronautical and space activities of the United States shall be conducted so as to contribute . . . to the expansion of human knowledge of phenomena in the atmosphere and space. The Administration shall provide for the widest practicable and appropriate dissemination of information concerning its activities and the results thereof."

— NATIONAL AERONAUTICS AND SPACE ACT OF 1958

NASA SCIENTIFIC AND TECHNICAL PUBLICATIONS

TECHNICAL REPORTS: Scientific and technical information considered important, complete, and a lasting contribution to existing knowledge.

TECHNICAL NOTES: Information less broad in scope but nevertheless of importance as a contribution to existing knowledge.

TECHNICAL MEMORANDUMS: Information receiving limited distribution because of preliminary data, security classification, or other reasons.

CONTRACTOR REPORTS: Scientific and technical information generated under a NASA contract or grant and considered an important contribution to existing knowledge.

TECHNICAL TRANSLATIONS: Information published in a foreign language considered to merit NASA distribution in English.

SPECIAL PUBLICATIONS: Information derived from or of value to NASA activities. Publications include conference proceedings, monographs, data compilations, handbooks, sourcebooks, and special bibliographies.

TECHNOLOGY UTILIZATION PUBLICATIONS: Information on technology used by NASA that may be of particular interest in commercial and other non-aerospace applications. Publications include Tech Briefs, Technology Utilization Reports and Notes, and Technology Surveys.

Details on the availability of these publications may be obtained from:

**SCIENTIFIC AND TECHNICAL INFORMATION DIVISION
NATIONAL AERONAUTICS AND SPACE ADMINISTRATION
Washington, D.C. 20546**

